The Journal of Experimental Biology 214, 4073-4081

doi:10.1242/jeb.047001

COMMENTARY

Damping in flapping flight and its implications for manoeuvring, scaling and evolution

Tyson L. Hedrick

University of North Carolina at Chapel Hill, Department of Biology CB #3280, Chapel Hill, NC 27599, USA

thedrick@bio.unc.edu

Accepted 27 September 2011

Summary

Flying animals exhibit remarkable degrees of both stability and manoeuvrability. Our understanding of these capabilities has recently been improved by the identification of a source of passive damping specific to flapping flight. Examining how this damping effect scales among different species and how it affects active manoeuvres as well as recovery from perturbations provides general insights into the flight of insects, birds and bats. These new damping models offer a means to predict manoeuvrability and stability for a wide variety of flying animals using prior reports of the morphology and flapping motions of these species. Furthermore, the presence of passive damping is likely to have facilitated the evolution of powered flight in animals by providing a stability benefit associated with flapping.

Supplementary material available online at http://jeb.biologists.org/cgi/content/full/214/24/4073/DC1

Key words: biomechanics, evolution, flight, manoeuvrability, stability.

Introduction

Flying animals exhibit surprising resistance to environmental perturbations given their small size and resulting small moments of inertia, a measure of their intrinsic resistance to turning. It is less surprising that flying animals are also highly manoeuvrable when compared with much larger flying machines, benefiting from these same differences in moment of inertia. Flying animals also possess a large suite of sensory systems that serve to gather information on their current state, enabling feedback control of position, orientation and derivatives of these quantities (Taylor and Krapp, 2007). In particular, gyroscopic sensors capable of providing information on turning rate to flying insects, first halteres (Pringle, 1948) and later antennae (e.g. Sane et al., 2007), have received much recent attention along with the responses of insects to imposed body rotations (Nalbach and Hengstenberg, 1994; Hinterwirth and Daniel, 2010) and integration of visual and mechanosensory systems (e.g. Bender and Dickinson, 2006).

These neurosensory systems and their resulting feedback connections to the flight motor systems enable active responses to perturbations and are required for flight control. However, recent work has shown that flapping flyers benefit from several types of passive stability (Hesselberg and Lehmann, 2007; Hedrick and Biewener, 2007; Hedrick et al., 2009; Cheng et al., 2010; Faruque and Humbert, 2010a; Dickson et al., 2010). These passive stability properties, the focus of this Commentary, both enhance resistance to perturbations and inhibit manoeuvres. The presence of these passive effects changes our understanding of the general model of animal flight stability and manoeuvrability from one where inertia is the only factor limiting turning and all stability is provided by neurosensory feedback to one where both inertia and damping must be considered and neurosensory control models must incorporate realistic damping, regardless of the size of the animal. In short, these passive stability models provide new insight into the basic determinants of animal flight dynamics.

Here, I review recent work on these models of passive damping, their effect on manoeuvrability and the predictions they make for the scaling of stability and manoeuvrability among flying animals, and consider how passive damping may have influenced the evolution of flapping flight. I then compare the predictions of the scaling of stability and manoeuvrability with the trends present in a data set gathered from prior studies of the morphology and flapping kinematics of insects, birds and bats. Examination of these results shows that stability and manoeuvrability characteristics do not scale as predicted by isometry despite the generally isometric scaling of morphology in flying animals; normalized measures of performance such as damping half-life in wingbeats vary more than predicted while dimensional quantities such as damping half-life measured in milliseconds vary less. This may reflect selective pressures related to maintaining adequate flight stability or may be a by-product of the need for animals to produce sufficient aerodynamic forces to support their weight in low speed flight. In either case, the results show that flapping simplifies some aspects of aerial stability and manoeuvrability regardless of the size of the animal, potentially facilitating the evolution of flapping flight from gliding precursors.

Manoeuvrability and stability

Examination of damping effects and other determinants of manoeuvrability and stability first requires a brief review of the relevant concepts and kinetics equations. In the most general sense, manoeuvrability may be defined as the ability of an animal to change its orientation or direction of travel, and stability as the ability to maintain these states (Dudley, 2002). For example, consider an insect in hovering flight (Fig. 1). Its average linear and angular velocities are, by definition of hovering, zero in all directions. However, a slight gust of wind might accelerate the insect, giving it a non-zero angular velocity in rotation to its left. If the insect slows down and reaches zero velocity following the perturbation, it is stable with respect to yaw velocity – its original

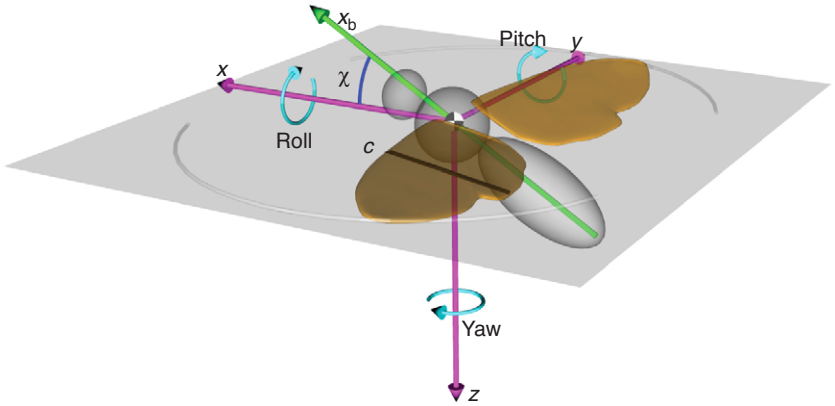

Fig. 1. A dorso-lateral view of an idealized hovering insect showing the three body segments, two wings with a chord length *c* shown on the near wing, the manoeuvring axes (*x*, *y* and *z*), the corresponding roll, pitch and yaw rotations, the centre of mass through which these axes pass, and the insect's longitudinal body axis x_b, offset for the manoeuvring axes by the free body angle χ. Using a set of manoeuvring axes that are aligned with gravity in the animal's standard flight posture simplifies analysis of the dynamics, at the cost of complicating the calculation of the moment of inertia.

state has been restored. If instead the animal's angular velocity stays constant following the perturbation, it is neutrally stable, i.e. neither stable nor unstable. If the animal's velocity increases following the initial perturbation, it is unstable. As manoeuvres are by definition a change in state, manoeuvrability may be thought of as both the animal's capacity to create a temporary self-perturbation and the magnitude of the resulting rate of state change.

Here, I focus on changes to the orientation of a flying animal (Fig. 1) rather than changes in position. A change in orientation may be brought about by application of a torque (τ) or by inertial reorientation as in a falling cat (Frohlich, 1980). A torque could be the result of purposeful manoeuvring produced by asymmetries in the animal's flapping motion or the result of an environmental factor such as a gust of wind. Regardless of the source, the torque will produce an angular acceleration ($\dot{\omega}$), the magnitude of which is determined by the magnitude of the torque and the animal's moment of inertia *I*. This acceleration results in angular velocity (ω), which will persist until either countered by the animal producing a torque of the opposite sign (–τ) or reduced to zero by damping torques intrinsic to the animal's motion. Thus:

$$I\dot{\omega} = \tau - C_{\omega}\omega\,, \qquad (1)$$

where C_{ω} is a damping constant resulting in a damping torque linearly proportional to the current angular velocity. This potentially represents either truly linear sources of friction or drag (e.g. Stokes drag), or a linear approximation to a non-linear effect such as conventional aerodynamic pressure drag. Thus, an animal with a large moment of inertia will experience less angular acceleration in response to a manoeuvring torque or environmental perturbation than an animal with a small moment of inertia. Hence, manoeuvrability and stability are commonly presented as opposites because a common factor, *I*, reduces the magnitude of the acceleration caused by both intended and unintended torques. The same may be said for damping, where larger damping coefficients are stabilizing and result in small net rotations for a given initial angular velocity but therefore also result in smaller changes in orientation following production of a manoeuvring torque.

Additionally, an animal with a large C_{ω} relative to *I* has dynamics dominated by damping effects whereas an animal with a larger *I* relative to C_{ω} has more inertial dynamics. This is the case because an animal with a relatively large *I* accelerates slowly from rest and takes longer to reach a speed where τ is equal to $C_{\omega}\omega$, regardless of the magnitude of the applied torque. An animal with relatively smaller *I* or larger C_{ω} more quickly reaches a speed where $C_{\omega}\omega=\tau$ and acceleration ceases. Thus, the relative importance of inertia and damping depends on both the magnitude of torque and the duration of its application. However, until recently it was commonly assumed that the damping portion of Eqn 1, $-C_{\omega}\omega$ was small relative to *I*, even for small animals (Ellington, 1984b; Fry et al., 2003). This is not the case, as was first shown in simple yaw turns and extended to other modes of animal flight. Instead of minimal damping caused only by body drag, animals experience substantial damping for certain manoeuvres as a result of interactions between body movement, wing movement and flapping flight aerodynamics, as described below.

Flapping counter torque in yaw turning

The most basic case for revealing the influence of flapping flight aerodynamics and damping on body dynamics lies in planar yaw turns where an animal in hovering or near-hovering flight and flapping with a horizontal stroke plane rotates about an axis through its centre of mass and parallel to gravity, executing what is essentially a two-dimensional manoeuvre. As the animal turns, its body rotation influences the velocity of the wings in the global coordinate system (i.e. relative to the fluid), resulting in global frame kinematic asymmetries even if wing motion is symmetric in the body coordinate system. These kinematic asymmetries produce force asymmetries between the right and left wings. The force asymmetries then lead to a net torque counter to the direction of body rotation. In the downstroke phase of a typical wingbeat cycle, the counter torque is provided by the outside wing, e.g. the left wing in an animal rotating to the left. In the upstroke phase, the counter torque is provided by the inside wing (Fig. 2).

The effect described above can be combined with equations for blade-element models of flapping flight – simplified mathematical models that depend only on wing morphology, kinematics and a predetermined function linking these variables to aerodynamic forces – to reach an analytic prediction for the magnitude of flapping counter torque (FCT) acting on a flapping flyer engaged in a planar yaw turn of the type described above. The derivation is explored in detail elsewhere (Hedrick et al., 2009; Cheng and Deng, 2010) and results in:

$$I\dot{\omega} = -\omega\rho R^4 \bar{c}\hat{r}_3^3(S)\Phi n\,\overline{C_D(d\hat{\phi}/d\hat{t})}\,, \qquad (2)$$

or, by combination of terms into a single damping constant C_{ω}:

$$I\dot{\omega} = -\omega C_{\omega}\,, \qquad (3)$$

where *I* is the animal's moment of inertia, $\dot{\omega}$ is angular acceleration, ω is angular velocity, ρ is air density, *R* is wing length, $\bar{c}$ is mean wing chord, $\hat{r}_3^3(S)$ is the cube of the third moment of wing area, Φ is flapping amplitude, *n* is flapping frequency, $\overline{C_D(d\hat{\phi}/d\hat{t})}$ is the stroke-average product of the aerodynamic drag coefficient and non-dimensional wing angular velocity, and C_{ω} is a coefficient combining all wing morphological and flapping kinematic terms at

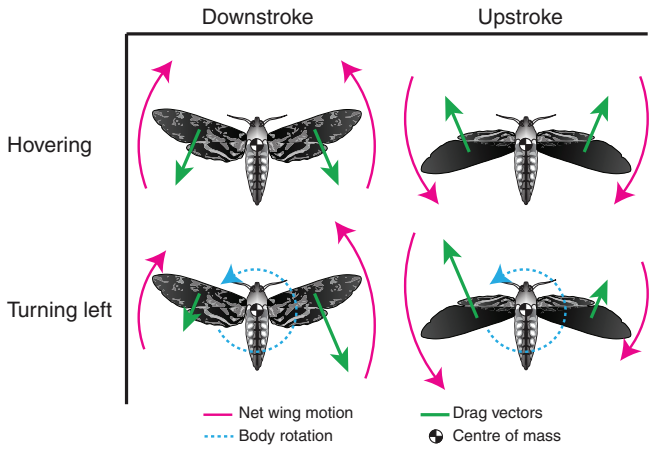

Fig. 2. This overhead view of a hawkmoth in hovering flight (top row) and yaw turning flight (bottom row) illustrates the flapping counter torque model. During hovering flight, the left and right wings produce net aerodynamic forces directed upward (lift) and opposite to the direction of wing motion (drag). Each wing also produces a torque about the centre of mass, but these torques oppose one another and result in no net torque in symmetric hovering. The upstroke case is identical save for the reversal of wing motion and corresponding change in the direction of drag. If the animal begins rotating to its left (bottom row), symmetric wing motion about the body results in asymmetric motion relative to the surrounding air. These kinematic asymmetries result in force asymmetries and left and right wing torques, which are no longer equivalent. In downstroke, the right side wing produces a greater drag and therefore there is a net torque to the right. In upstroke, the left wing produces more drag and the net torque remains directed to the right, opposing the turning motion.

standard air pressure. As in Hedrick et al. (Hedrick et al., 2009), all animals were assumed to have identical aerodynamic force coefficients and non-dimensional wing kinematics, with $\overline{C_D(d\hat{\phi}/d\hat{t})}$ equal to 6.0. This model predicts a damping torque linear with respect to angular velocity despite the intrinsic non-linear relationship between force and velocity for solid objects interacting with fluids at high Reynolds number.

In Hedrick et al. (Hedrick et al., 2009), a prediction of the decay half-life ($t_{1/2}$), the time taken for a decelerating animal to reach half its initial angular velocity, was used as a means of matching the FCT model to experimental recordings and comparing the effects of damping in different species. Half-life in seconds, $t_{1/2}(t)$ is given by:

$$t_{1/2}(t) = \frac{\ln(2)I}{C_\omega} \,. \tag{4}$$

Next, I consider the scaling of FCT damping, or how damping might be expected to change with size in flying animals. The wing and body dimensions of flying animals are commonly found to scale isometrically or nearly so, with flapping frequency inversely proportional to wing length (Greenewalt, 1962). In this case and assuming no variation in aerodynamic force coefficients, flapping amplitude or non-dimensional wing angular velocity with body size, C_ω is expected to scale as $M_b^{4/3}$ while $I \propto M_b^{5/3}$ and, thus, $t_{1/2}(t) \propto M_b^{1/3}$, showing that damping half-life is predicted to increase with increasing body size.

Hedrick et al. (Hedrick et al., 2009) also showed that non-dimensional half-life, $t_{1/2}(\hat{t})$ or half-life in wingbeats, given as:

$$t_{1/2}(\hat{t}) = \frac{\ln(2)In}{C_\omega} \,, \tag{5}$$

is expected to scale as M_b^0. Thus, the turning dynamics of isometrically scaled animals should be the same when expressed in units of number of flaps rather than time.

As noted by Dickson et al. (Dickson et al., 2010), FCT damping and the associated dynamics equations may also be fully non-dimensionalized, allowing more direct comparisons of damping coefficients among animals and dynamically scaled models. The non-dimensional versions are:

$$\hat{I} = \frac{I}{\rho \bar{c}^5} \,, \tag{6}$$

$$\hat{\omega} = \frac{\omega}{n} \,, \tag{7}$$

$$\hat{\dot{\omega}} = \frac{\dot{\omega}}{n^2} \,, \tag{8}$$

$$\hat{C}_\omega = \frac{C_\omega}{\rho \bar{c}^5 n} \,, \tag{9}$$

$$\hat{I}\hat{\dot{\omega}} = -\hat{C}_\omega \hat{\omega} \,, \tag{10}$$

$$\hat{\tau} = \frac{\tau}{\rho \bar{c}^5 n^2} \,, \tag{11}$$

where a circumflex indicates a non-dimensional quantity.

The FCT model was supported using Eqn 4 to successfully predict rates of angular deceleration in seven species of flying animal for which detailed yaw turning kinematics were available (Hedrick et al., 2009). Recent work on fruit flies, including analysis of saccade turns in a dynamically scaled model (Cheng et al., 2010) and in free flight (Bergou et al., 2010), free-flight aerial perturbation experiments (Ristroph et al., 2010) and a linear dynamics analysis of the manoeuvring torques generated by wing asymmetries (Dickson et al., 2010) have further emphasized the importance of FCT-like effects to animal flight dynamics.

Extensions to flapping counter torque

The basic FCT model predicts rates of deceleration for animals flapping symmetrically while engaged in a planar yaw turn. This generalizes to rotations about the axis perpendicular to the stroke plane of the animal. For example, Hedrick and Biewener (Hedrick and Biewener, 2007) used an FCT-like model to explain the roll dynamics of cockatoos engaged in slow forward flight and flapping with a stroke plane nearly perpendicular to the roll axis.

Flapping counter torque-like effects also occur along other rotational and linear axes aside from those perpendicular to the stroke plane. Faruque and Humbert (Faruque and Humbert, 2010b) showed how sideslip motion of a hovering fruit fly changes the flow vectors over the wings and leads to a net damping force which reduces sideslip velocity. Cheng and Deng (Cheng and Deng, 2010) using a mechanical flapper and modelling approach, provide analytical approximations for wing flapping and body dimensions for all six degrees of freedom in hover and slow flight, including FCT-like effects for roll, pitch and yaw and flapping counter force (FCF) effects for translational motions. Thus, although most apparent in yaw turns through the stroke plane, FCT-like models help explain other stability and instability modes for flying animals. Recent free-flight recordings of forward flight in fruit flies (Ristroph et al., 2011) and linear accelerations in hawkmoths (Cheng et al., 2011) provide experimental support for the importance of flapping-related damping in other flight modes.

The underlying blade-element analytical approximation of flapping flight used to develop the FCT damping model also predicts that actively generated torques resulting from wing motion asymmetries in the body coordinate system should vary linearly with the magnitude of the asymmetry (Hedrick et al., 2009). This was demonstrated experimentally by Dickson and colleagues (Dickson et al., 2010) using a dynamically scaled fruit fly model, and the combination of linear damping and linear actuation used to show how fruit flies respond to control inputs of different time scales.

FCT model predictions

The FCT damping model described above leads to several predictions of how damping should relate to body size in flying animals. Firstly, given the near-isometric scaling of flying animals, the model predicts that the strength of damping will be a linear function of flapping frequency. Therefore, the model also predicts that animals of different sizes will have similar damping quantities when damping is expressed in wingbeats rather than time, i.e. as a reduction in angular velocity per flap rather than per second. Flapping frequency itself is predicted to scale as wing length ($n \propto R^{-1}$) or as $M_b^{1/3}$ for isometric animals through application of muscle models (Hill, 1950) and damped oscillator models based on wing inertia and idealized spring-like muscles (Sotavalta, 1952; Greenewalt, 1960). The combination of isometric FCT damping and flapping frequency results in a prediction that damping in an absolute sense decreases with body size. Normalized damping on a per-wingbeat time scale is potentially important, but so too is damping on an absolute scale. Large and less damped animals might need to respond to perturbations or initiate manoeuvres mid-wingbeat while small and heavily damped animals might allow damping to mitigate the effects of a perturbation before responding, as was found in fruit flies (Ristroph et al., 2010).

The aforementioned damping predictions are rooted in assumptions of similar flapping kinematics and isometric scaling among species. Both these assumptions run foul of observations and measurements of animals. For instance, many birds are known to reduce their wing area during upstroke, which is likely to reduce aerodynamic damping during that phase of the stroke cycle. Additionally, while the body proportions of flying animals do scale isometrically or nearly so (Greenewalt, 1962; Van den Berg and Rayner, 1995; Dudley, 2000), the blade-element equation for aerodynamic lift (Weis-Fogh, 1973) used as the basis of the FCT model does not predict a constant lift to weight ratio in hovering flight. Blade-element lift is given by:

$$L = 2\tfrac{1}{8}\rho R^3 \bar{c} \hat{r}_2^2(S) \Phi^2 n^2 \overline{C_L (\mathrm{d}\hat{\phi}/\mathrm{d}\hat{t})^2}\ , \qquad (12)$$

where L is the total lift from the left and right wings, $\hat{r}_2(s)$ is the second moment of wing area and $\overline{C_L}$ is the average coefficient of lift. Under isometric scaling, Eqn 12 predicts that $L \propto M_b^{2/3}$, implying that larger animals cannot produce enough lift support their own weight. This is clearly not so; small deviations from isometry or systematic variation in aerodynamic force coefficients or flapping kinematics may counter this adverse scaling effect in large flying animals. In either case, it is not clear what impact the variation might have on the predicted scale related changes in FCT damping. In the following section, I resolve these questions surrounding the scaling of damping and flight forces and the adequacy of simple blade-element models by comparing the predictions described above with data gathered from numerous prior studies of flying animals.

Broad application of the FCT model

In principle, because the FCT model requires only a few measurements of kinematics, wing morphology and overall moment of inertia, it offers a new means of assessing the manoeuvrability and stability of a wide variety of flying animals beyond those for which detailed manoeuvring kinematics have been measured. In practice, the set of animals for which all of these quantities have been characterized is not large, with moment of inertia most rarely measured. Thus, the first task in broadly applying models of manoeuvrability or stability to flying animals is investigation of trends in moment of inertia, the quantity measuring resistance to an object's change in orientation.

Moment of inertia

Prior work on variation in moment of inertia in bats (Thollesson and Norberg, 1991) reported it to be isometric with respect to both body mass and wing length, i.e. $I \propto M_b^{5/3}$ and $I \propto R^5$. A similar study of moment of inertia in birds found it to be isometric with respect to wing length but not body mass (Van den Berg and Rayner, 1995). Both of these studies examined roll moment of inertia of the animal in a posture with the wings outstretched. In this case, the whole-animal moment of inertia is dominated by the inertia of the wings, making roll and yaw moments of inertia similar and much greater than pitch inertia. Similar measurements of insects are less common and the results more varied (Ellington, 1984a), in part due to variation in insect wing shape but also because the wings of insects contribute less to total moment of inertia than in birds and bats (Dudley, 2000). Here, an inertia model capable of incorporating information collected on insect wing moments of inertia for rotations about the base (see Appendix and supplementary material Tables S1 and S2) was applied to estimate I for a data set of 42 insects, bats and birds (supplementary material Table S1). This revealed a slight and non-significant positive allometric scaling of I with respect to body mass (Table 1), supporting the initial prediction that FCT stability decreases with increases in body size.

Other FCT parameters: wing length, shape and flapping frequency

In addition to moment of inertia, wing length also features prominently in the FCT model; it scales with slight positive but again non-significant allometry in the data set of flying animals used here (Table 1). Flapping frequency n was found to scale at slightly but not significantly less than predicted as either a function of wing length R or body mass M_b (Table 1).

Along with moment of inertia, the non-dimensional second [$\hat{r}_2(S)$] and third [$\hat{r}_3(S)$] moments of wing area are rarely reported in studies of flying animals, although they may be recovered from accurate reproductions of wing planforms such as those provided in Sotavalta (Sotavalta, 1952). Fortunately, these non-dimensional moments of area vary little among species and have only a modest effect on the strength of damping or lift production (Weis-Fogh, 1973; Ellington, 1984a). In cases where they were not reported for a species with otherwise complete data, the mean value for this data set, 0.59 for $\hat{r}_3(S)$ and 0.54 for $\hat{r}_2(S)$, was substituted (supplementary material Table S1).

Damping half-life

Despite broad agreement between the aforementioned morphological and kinematic parameters – the components determining FCT effects – and isometric predictions, FCT damping half-life in milliseconds scaled with negative allometry, increasing as $M_b^{0.17}$, significantly different from the $M_b^{1/3}$ scaling predicted by

Table 1. Scaling of damping parameters

x	y	r^2	B_{iso}	B_{model1}	B_{RMA}	s.e.
R	M_b	0.92	0.33	0.36	0.38*	0.02
$\bar{c}$	M_b	0.86	0.33	0.38*	0.41*	0.02
I_{wing}	M_b	0.93	1.67	1.80	1.87*	0.08
I	M_b	0.99	1.67	1.72	1.73*	0.03
Φ	M_b	0.03	0.00	0.02	0.10*	0.02
n	M_b	0.53	–0.33	–0.27	–0.37	0.04
n	R	0.77	–1.00	–0.86	–0.98	0.08
L	M_b	0.96	0.67	0.94*	1.04*	0.03
$t_{1/2}(t)$	M_b	0.38	0.33	0.17*	0.27*	0.03
$t_{1/2}(\hat{t})$	M_b	0.06	0.00	–0.11	–0.41*	0.06
$\hat{C}_\omega$	M_b	0.05	0.00	–0.09	–0.41*	0.06

Results for regressions on log-transformed data; hence, $y=Ax^B$. Model 1 and reduced major axis (RMA) slopes are provided. In comparisons of directly measured physical variables, B_{RMA} is likely to better capture the relationship between the parameters. However, in comparison of derived variables such as $t_{1/2}(t)$ and $\hat{C}_\omega$, substantially greater error is expected in the dependant variable and B_{model1} may be more appropriate. Slopes significantly different from isometry ($P<0.05$, two-sided t-test) are indicated with an asterisk.

R, wing length; $\bar{c}$, mean wing chord; I, moment of inertia; Φ, flapping amplitude; n, flapping frequency; L, total lift from the left and right wings; $t_{1/2}(t)$, half-life in seconds; $t_{1/2}(\hat{t})$, non-dimensional half-life; $\hat{C}_\omega$, non-dimensional FCT damping coefficient.

isometry (Fig. 3A, Table 1). Similarly, FCT damping half-life in wingbeats was predicted to be constant among animals of different body sizes, but was found to scale with slight and not significant negative allometry with respect to body mass (Fig. 3B). In summary, allometric scaling of wing length, wing chord, flapping amplitude and frequency partially counters the expected decrease in FCT effects with body size. The strength of damping in dimensional terms does decline with body size, but at approximately half the rate predicted.

Blade-element lift

Similar to FCT damping effects, lift as calculated from the blade-element force model underlying the FCT model did not scale as expected under isometry despite the isometric or nearly isometric scaling of many of its components, including wing length and flapping frequency. Instead of scaling at or close to $M_b^{2/3}$, lift from Eqn 12 scaled at $M_b^{0.94}$ and was not significantly different from $M_b^{1.0}$ (Table 1). While this must be the case, i.e. flying animals are clearly able to support their weight, it does not follow that the unmodified blade-element equations would provide an adequate model. However, the model was adequate for these data, indicating that no systematic adjustment is required to explain weight support for hovering or slow flying animals across the observed 5 order of magnitude body mass range. Had blade-element lift scaled as predicted by isometry and not equivalent to body mass, this would imply defects in the underlying FCT assumptions or a requirement that the coefficients of lift and drag systematically vary with size. As this was not the case, no overall adjustments are required.

Consequences of damping for manoeuvres

The differences in damping properties among species affect not only the dynamics of an animal following a manoeuvre or external perturbation but also the initiation of a manoeuvre when the animal uses wing asymmetries to create torques. As the animal enters into the manoeuvre and increases its angular velocity, damping produces torque in the opposite direction; if the manoeuvring kinematic is maintained for a sufficient time, the magnitude of FCT damping will match the manoeuvring torque of the animal and it will no longer accelerate. As shown in Dickson et al. (Dickson et al., 2010), the number of wingbeats required to reach this saturation point depends on the ratio of non-dimensional inertia $\hat{I}$ and non-dimensional FCT damping coefficient $\hat{C}_\omega$. Animals with a relatively large damping coefficient reach saturation more quickly, i.e. they more rapidly reach a velocity where the damping torque is equal to the input torque and cease accelerating. This, in turn, determines whether the dynamics of a particular manoeuvre are more strongly influenced by the animal's inertia or by damping and whether a first or second order control strategy is more appropriate (Cowan and Fortune, 2007). Furthermore, depending on the time scale of the manoeuvre in question, either inertia or damping may predominate. For example, manoeuvres that occur over many wingbeats will tend toward saturation and therefore be more influenced by damping than inertia, while short manoeuvres over a few wingbeats that do not approach saturation will be dominated by inertia. Manoeuvres in these different regimes demand different actuation and control strategies from the neurosensory and neuromuscular systems. For example, modulation of muscle activity and aerodynamic torque at an inertially dominated time scale leads to acceleration, but modulation at a time scale where damping dominates produces velocity.

To illustrate some of these differences, consider the predicted response of the fruit fly (*Drosophila melanogaster)* and hawkmoth (*Manduca sexta*) during a manoeuvre of identical non-dimensional time scale and magnitude $\hat{\tau}$. The manoeuvre is modelled here as a torque that first accelerates the animal in a leftward rotation and then, over the course of 15 wingbeats, switches to accelerating the animal to the right and then back to the left. The general case of such a sinusoidally varying torque is given by:

$$\hat{\tau}(\hat{t}) = \cos(2\pi\hat{t}\hat{f}_\tau^*) , \quad (13)$$

where $\hat{t}$ is non-dimensional time ($\hat{t}=tn$) and $\hat{f}_\tau^*$ is the non-dimensional torque stimulus frequency, given by:

$$\hat{f}_\tau^* = \frac{f_\tau}{n} , \quad (14)$$

i.e. the torque stimulus frequency, f_τ^* divided by the flapping frequency of the animal; 1/15 in the case described above.

Application of this manoeuvring torque to the animal produces the following dynamics:

$$\hat{I}\dot{\hat{\omega}}(\hat{t}) = -\hat{C}_\omega\hat{\omega}(\hat{t}) + \cos(2\pi\hat{t}\hat{f}_\tau^*) . \quad (15)$$

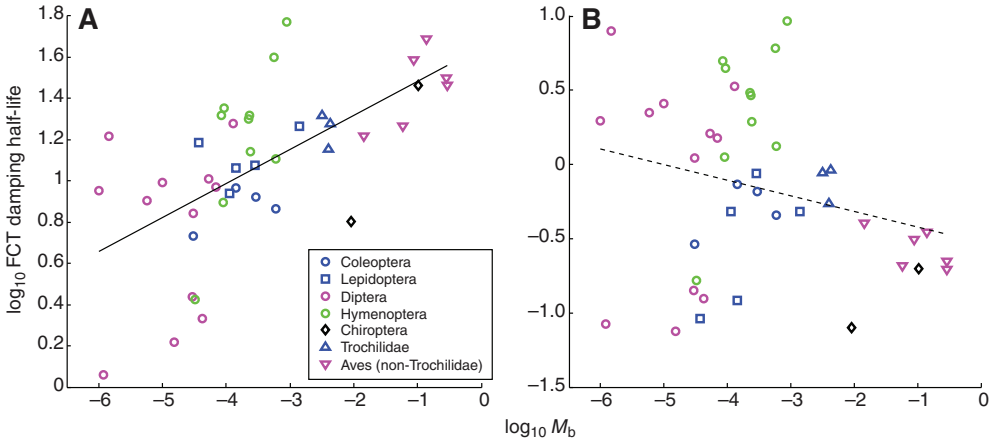

Fig. 3. These scatterplots show the predicted flapping counter torque (FCT) damping half-life in (A) milliseconds and (B) wingbeats ($\hat{t}$) *vs* body mass (kg) for 42 species of insects, birds and bats calculated using Eqns 4 and 5 applied to the data in supplementary material Table S1. Inertia was calculated following the model described by Eqns A1–A6 in the Appendix. The linear (model 1) regression line in A is significantly less than that predicted by isometric scaling (see Table 1). The dashed linear regression line in B is not significantly different from isometry.

In this example, with an $\hat{f}_\tau$ of 1/15, the less damped and more inertially governed fruit flies experience smaller angular velocity amplitudes and a greater phase lag between input torque and body velocity than the more heavily damped hawkmoth, which responds (in the non-dimensional time scale) more quickly to the input torque (Fig. 4). Because these differences are time scale dependent, with longer time scales enhancing damping effects and shorter time scales increasing the importance of inertia, to better compare the properties of different species, the input torque oscillation frequency predicted to result in a 45 deg phase lag between manoeuvring torque input and the animal's angular velocity, $\hat{f}_{45}$, was computed as:

$$\hat{f}_{45} = \pi \frac{In}{C_\omega} . \quad (16)$$

Aside from a difference in constants, $\hat{f}_{45}$ is identical to $t_{1/2}(\hat{t})$ (Eqn 5) and thus scales similarly. This 45 deg phase lag balances the inertial and damping effects on manoeuvrability (Dickson et al., 2010) and, for fruit flies, is close to the reported 10 wingbeat time scale for free-flight saccade manoeuvres (Fry et al., 2003). It is not clear that all flying animals operate at a midpoint between inertial and aerodynamic effects; Hedrick and Robinson (Hedrick and Robinson, 2010) report yaw turns of five wingbeats in *M. sexta*, a time scale predicted to result in a phase lag of 23 deg and dominated by damping. Nevertheless, $\hat{f}_{45}$ forms a convenient reference point for comparison of the flapping time scales relevant to manoeuvring in different species. These intrinsic manoeuvring time scales varied from 0.3 wingbeats in the crane fly *Tipula obsoleta* to 42 in the bumblebee *Bombus terrestris* in the data presented here (supplementary material Table S2). Thus, the degree to which inertia and damping determine the turning dynamics of animals appears to vary widely among species.

Damping, stability and the evolution of flapping flight

Flapping counter torque and similar flapping-related damping effects add a new dimension to scenarios describing the evolution of powered flight in animals, which must explain the evolution of wings to provide lift and flapping motions to provide thrust. Different scenarios account for the appearance of these components in different ways and orders. For example, the recent discovery of controlled parachuting in ants with only minimal aerodynamic surfaces (Yanoviak et al., 2005) supports a scenario where aerial escape behaviour evolves first, leading to selection

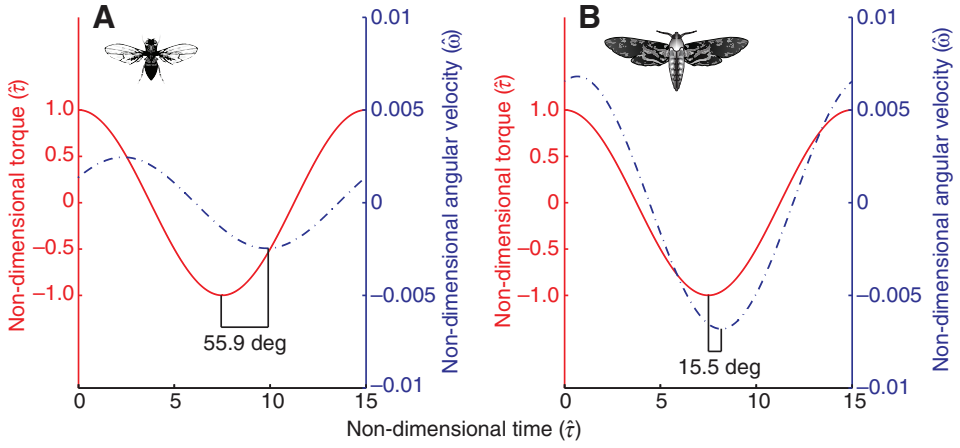

Fig. 4. This figure shows the manoeuvring response predicted for (A) a fruit fly (*Drosophila melanogaster*) and (B) a hawkmoth (*Manduca sexta*) following the same non-dimensional torque input with a non-dimensional frequency $\hat{f}_\tau$ of 1/15. The manoeuvring torque is periodic over a 15 wingbeat cycle; at that stimulation frequency the fruit fly's velocity is delayed by 56 deg with respect to the input. The hawkmoth, with its smaller inertia to damping ratio, has a phase delay of only 16 deg. At this non-dimensional time scale the fruit fly dynamics are influenced by inertia and damping but the hawkmoth is dominated by damping effects. The time scale in question, with a unidirectional turning torque applied over 7.5 wingbeats, is slightly faster than the reported time course of fruit fly saccades and slightly slower than the time course of yaw turns in *M. sexta*.

for better aerodynamic performance *via* the expansion of the aerodynamic surfaces and eventually to flapping wings, i.e. evolution of powered flight from gliding. A variant of the gliding scenario for the evolution of insect flight suggests that wings might first have evolved as sails to enable water surface skimming behaviour, with flapping evolving later to provide additional thrust along the water (Marden and Kramer, 1994). The wing-assisted inclined running scenario for the evolution of bird flight reverses the common order of wings first, then flapping by showing that oscillating forelimb motions help extant birds escape up steep inclines (Dial, 2003), by providing both additional traction and, with further wing development, aerodynamic thrust (Tobalske and Dial, 2007). Of the three scenarios just mentioned, flapping initially evolves as an afterthought to gliding, as a source of propulsion, or as a source of stability, respectively. Flapping counter torque-like effects provide another avenue by which flapping may evolve initially to provide stability, but in a gliding rather than terrestrial context.

The aforementioned possibility – that flapping might evolve to help stabilize gliding rather than to provide thrust or a direct locomotor benefit – would be most likely in gliding animals with poor stability. Certain modes of stability are easily provided for in gliding, but others are not. A drag-producing structure extending behind the body of the animal can provide passive yaw and pitch stability (Wootton and Ellington, 1991; Thomas and Taylor, 2001), but will not stabilize roll without active control of its position. In human-engineered fixed wing gliders, roll stability is provided by positioning the wings with a slight dihedral angle and by lift-based roll damping. A dihedral angle, or upward tilt to the wings, provides for roll stability by coupling sideslip (lateral motion of the body) with roll. Given a positive dihedral, a sideslip to the right would create a roll torque to the left. As roll causes sideslip by reorienting the aerodynamic force vectors of the wings, a dihedral angle stabilizes roll in any perturbation where the dihedral angle is greater than the roll perturbation. Roll damping influences roll velocity directly because non-zero roll rate to one side increases the effective angle of attack (α) of that wing, increasing the lift produced and therefore providing a restoring torque (Stengel, 2004). Both of these mechanisms increase in strength with wing size, due both to increases in total aerodynamic force and because larger wings produce forces at a greater distance from the centre of mass and thus have a greater moment arm. This means that the gliders least able to take advantage of fixed wing roll damping or dihedral effects and most in need of stability enhancement are those with small wings. Stability in such an animal may be improved by either (A) enlargement of the wing or (B) flapping and taking advantage of FCT-like damping. Following development of flapping to provide stability, enlargement of the wings and refinement of flapping kinematics may then lead to improved aerodynamic performance in both stability and thrust production (Fig. 5).

This FCT-enabled scenario for the evolution of flapping flight (Fig. 5) suggests a possible bifurcation in the evolution of flapping from gliding, where gliding animals that improve stability *via* larger wings rather than flapping then gain fewer benefits from flapping and may be less likely to evolve the necessary but potentially expensive musculature and motor control for fully powered flight. Thus, one solution to stability in gliding flight results in an evolutionary pitfall or local optima less likely to lead to the evolution of flapping flight. This may partially account for the diversity of gliding organisms compared with the paucity of groups in which flapping flight appeared.

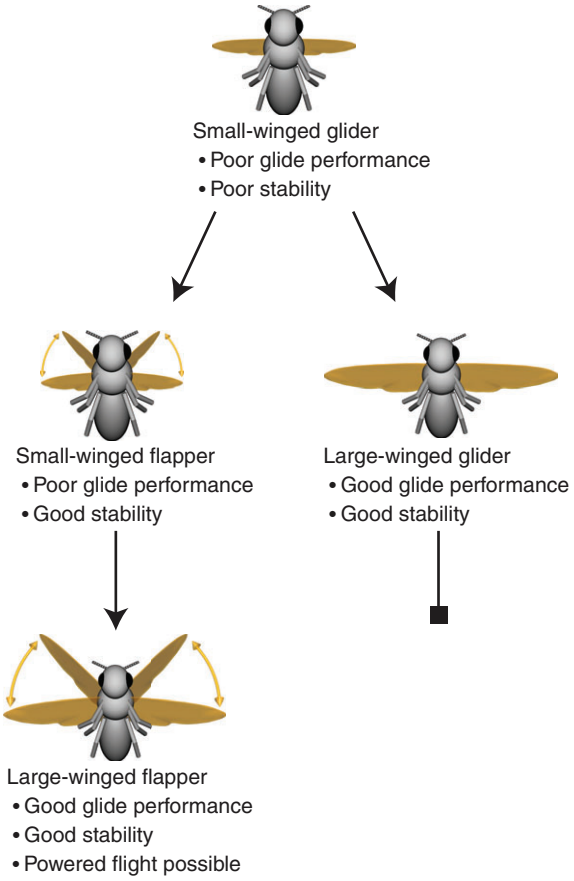

Fig. 5. This figure shows a possible scenario for the evolution of flapping flight from a gliding precursor taking stability into account. Small winged gliders have poor stability characteristics because they experience small benefits from a dihedral angle and roll damping. Further, use of a dihedral angle reduces glide performance by re-orienting lift slightly inward on each wing. Both flapping and an increase in wing size could improve flight stability. Flapping with small wings increases stability and may marginally improve gliding performance by helping the animal stay on course; further improvements in glide performance may be gained through increasing wing size. In contrast, increasing wing size from a small-winged ancestral starting point improves stability and glide distance, potentially leading to a local evolutionary optima where the addition of flapping provides little benefit while requiring investment in additional muscle and neural control resources.

Future work

Although much recent progress has been made toward understanding the factors influencing the flight dynamics of animals, many more questions remain. These form two general classes: (A) improving, extending and validating the underlying models and (B) understanding their biological implications for the neural control of motion, behaviour, ecology and evolution. With respect to the former, a substantial challenge lies in extending the simple analytic equations predicting dynamics in two-dimensional yaw turns at hover to more complex manoeuvres in different flight conditions, and validating these extensions *via* free-flight experiments with live animals. Similarly, the biological implications of the dimensional and non-dimensional damping parameters of different animals are unknown, as is the extent to which animal flight control strategies take advantage of FCT-like damping and linearities in torque production in different cases.

Appendix

Moment of inertia

The moment of inertia strongly influences the turning dynamics of flying animals, but is rarely reported as a whole-animal quantity in morphometric studies, making it necessary to estimate it from other measurements. Here, I show how it was calculated in this Commentary. Much of the published information on moment of inertia for flying animals describes the moment of inertia of the wings rotating about the hinge rather than for the body as a whole (Sotavalta, 1952; Sotavalta, 1954; Van den Berg and Rayner, 1995). Taking advantage of this information requires a slightly unusual approach. Here, I model the body of the animal as a prolate spheroid with a minor radius 2/5 the length of the major radius. Body volume was computed from body mass by assuming a density of $1\,\mathrm{g\,cm^{-3}}$ (that of water) and used to compute the minor radius of the spheroid as follows:

$$b = \frac{2}{5}\sqrt{\frac{\frac{3}{4}V_\mathrm{b}}{\pi\left(\frac{2}{5}\right)^2}}\,, \qquad \text{(A.1)}$$

where V_b is body volume and b is the minor radius of the spheroid. The moment of inertia of such a spheroid about its major and minor axes is:

$$I_{aa} = \frac{2}{5}M_\mathrm{b}b^2\,, \qquad \text{(A.2)}$$

$$I_{bb} = \frac{1}{5}M_\mathrm{b}(a^2 + b^2)\,, \qquad \text{(A.3)}$$

where I_{aa} is the moment of inertia for rotation about the major axis, I_{bb} the moment of inertia for rotation about the minor axis, M_b is body mass and a and b are the major and minor axis radii, respectively. In slow flight, animals typically adopt an upwardly tilted body angle, affecting moment of inertia for rotations about an axis parallel to gravity. A 30 deg angle was assumed here; the corrected moment of inertia is given by:

$$I_{zz} = \sin(\chi)^2 I_{aa} + \cos(\chi)^2 I_{bb}\,, \qquad \text{(A.4)}$$

where χ is the pitch angle of the animal. Wing moments of inertia (I_wing) are typically reported in the literature as the moment of inertia for rotation about the wing root, not about the centre of mass of the animal, the case of interest here. Without additional data on the mass distribution within the wing, it is not possible to exactly calculate the relevant whole-animal I, but it may be closely approximated by the radius of a point mass with the same mass and moment of inertia of the wing extended by the radius of the body, or the minor radius of the spheroid in this case:

$$I_{\mathrm{wing}'} = M_\mathrm{w}\left(\sqrt{\frac{I_\mathrm{wing}}{M_\mathrm{w}}} + b\right)^2\,, \qquad \text{(A.5)}$$

where $I_{\mathrm{wing}'}$ is the inertia of an outstretched wing rotating about an axis through the centre of mass of the animal and parallel to gravity. Thus, the complete estimated moment of inertia of the animal for a yaw rotation, referred to as I for the remainder of this paper is:

$$I = I_{zz} + 2I_{\mathrm{wing}'}. \qquad \text{(A.6)}$$

This moment of inertia model was chosen from a number of possibilities because it provides, *via* the spheroid minor axis, a better approximation of the distance between the wing root and centre of mass when compared with cases for which these data have been collected (Thollesson and Norberg, 1991; Hedrick et al., 2009). Finally, unlike some earlier inertia models such as that of Ellington (Ellington, 1984a), added mass (the mass of fluid accelerated along with the wing) was not included in these calculations of whole-animal inertia because fluid forces are accounted for separately in the blade-element models of wing forces. Including added mass in the inertia model would incorporate the same phenomena twice.

Glossary

Blade-element aerodynamic force model
A mathematical model of aerodynamic force production from a wing that divides the wing into a series of strips along the base to tip axis. The forces applied to each strip are then calculated from air density, the velocity of the strip, its aerodynamic force coefficients and area. The forces from all strips are then summed (or integrated in analytic rather than numeric blade-element models) to give the total force produced by the wing. Blade-element models can take into account different wing shapes and different flow conditions along a wing caused by flapping and are amenable to analytic solutions. They do not include a fluid model or any notion of the time history of aerodynamic forces, and depend on aerodynamic force coefficients from experiments or other sources.

Isometric scaling
A case in which changes in overall size do not produce changes in the relative proportions. For instance, the surface area of a sphere is proportional to the square of its radius regardless of the size of the sphere. Animals that exhibit isometric scaling may be referred to as geometrically similar.

Moment of inertia
A measure of an object's resistance to rotation. The role of moment of inertia for rotational motion is analogous to the role of mass in linear motion.

Torque
A measure of rotational force; the role of torque in rotational motion is analogous to that of force in linear motion.

Passive damping
Used here to refer to effects that cause reductions in the current rotational or linear velocity of an animal without requiring any particular action on the part of the animal beyond locomotor movements necessary for steady activity.

Stability
Used here to refer to the tendency of an animal to return to a standard state (e.g. hovering) from a perturbed state (e.g. turning to the left).

List of symbols and abbreviations

a	spheroid major axis
b	spheroid minor axis
$\bar{c}$	mean wing chord
C_D	coefficient of drag
C_L	coefficient of lift
C_ω	FCT damping coefficient
$\hat{C}_\omega$	non-dimensional FCT damping coefficient
$\hat{f}_{45}$	non-dimensional input torque frequency which produces a 45 deg phase lag
f_τ	input frequency of manoeuvring torque
$\hat{f}_\tau$	non-dimensional input frequency of manoeuvring torque
I	moment of inertia for a yaw rotation
FCT	flapping counter torque
$\hat{I}$	non-dimensional moment of inertia for a yaw rotation
L	lift
M_b	body mass
M_w	wing mass
n	flapping frequency
$\hat{r}_2(S)$	non-dimensional second moment of wing area
$\hat{r}_3(S)$	non-dimensional third moment of wing area
R	wing length
t	time
$\hat{t}$	non-dimensional time
V_b	body volume

x_b	body longitudinal (x) axis
α	angle of attack
ρ	air density
τ	torque
$\hat{\tau}$	non-dimensional torque
Φ	flapping amplitude
χ	pitch angle
ω	yaw angular velocity
$\hat{\omega}$	non-dimensional yaw angular velocity
$\dot{\omega}$	yaw angular acceleration
$\hat{\dot{\omega}}$	non-dimensional yaw angular acceleration

Acknowledgements

I wish to thank Brad Dickerson for helping compile the data tables and Jim Usherwood, María José Fernández and two anonymous referees for comments and discussion.

Funding

This work was funded by NSF IOS-0920358 to T.L.H.

References

Bender, J. A. and Dickinson, M. H. (2006). A comparison of visual and haltere-mediated feedback in the control of body saccades in *Drosophila melanogaster*. *J. Exp. Biol.* **209**, 4597-4606.

Bergou, A. J., Ristroph, L., Guckenheimer, J., Cohen, I. and Wang, Z. J. (2010). Fruit flies modulate passive wing pitching to generate in-flight turns. *Phys. Rev. Lett.* **104**, p. 148101.

Cheng, B. and Deng, X. (2010). Mathematical modelling of near-hover insect flight dynamics. *ASME Conf. Proc.* **2010**, 197-206.

Cheng, B., Fry, S. N., Huang, Q. and Deng, X. (2010). Aerodynamic damping during rapid flight maneuvers in the fruit fly *drosophila*. *J. Exp. Biol.* **213**, 602-612.

Cheng, B., Deng, X. and Hedrick, T. L. (2011). The mechanics and control of pitching manoeuvres in a freely flying hawkmoth (*Manduca sexta*). *J. Exp. Biol.* **214**, 4092-4106.

Cowan, N. J. and Fortune, E. S. (2007). The critical role of locomotion mechanics in decoding sensory systems. *J. Neurosci.* **27**, 1123-1128.

Dial, K. P. (2003). Wing-assisted incline running and the evolution of flight. *Science* **299**, 402-404.

Dickson, W. B., Polidoro, P., Tanner, M. M. and Dickinson, M. H. (2010). A linear systems analysis of the yaw dynamics of a dynamically scaled insect model. *J. Exp. Biol.* **213**, 3047-3061.

Dudley, R. (2000). *The Biomechanics of Insect Flight. Form, Function, Evolution*. Princeton, NJ: Princeton University Press.

Dudley, R. (2002). Mechanisms and implications of animal flight maneuverability. *Integr. Comp. Biol.* **42**, 135-140.

Ellington, C. P. (1984a). The aerodynamics of hovering insect flight. II. Morphological parameters. *Phil. Trans. R. Soc. Lond. B* **305**, 41-78.

Ellington, C. P. (1984b). The aerodynamics of hovering insect flight. III. Kinematics. *Phil. Trans. R. Soc. Lond. B* **305**, 41-78.

Faruque, I. and Humbert, J. S. (2010a). Dipteran insect flight dynamics. Part 1, longitudinal motion about hover. *J. Theor. Biol.* **264**, 538-552.

Faruque, I. and Humbert, J. S. (2010b). Dipteran insect flight dynamics. Part 2, lateral-directional motion about hover. *J. Theor. Biol.* **265**, 306-313.

Frohlich, C. (1980). The physics of somersaulting and twisting. *Sci. Am.* **242**, 154-164.

Fry, S. N., Sayaman, R., and Dickinson, M. H. (2003). The aerodynamics of free-flight maneuvers in *Drosophila*. *Science* **300**, 495-498.

Greenewalt, C. H. (1960). The wings of insects and birds as mechanical oscillators. *Proc. Am. Philos. Soc.* **104**, 605-611.

Greenewalt, C. H. (1962). Dimensional relationships for flying animals. *Smithson. Misc. Collns.* **144**, 1-46.

Hedrick, T. L. and Biewener, A. A. (2007). Low speed maneuvering flight of the rose-breasted cockatoo (*Eolophus roseicapillus*). I. Kinematic and neuromuscular control of turning. *J. Exp. Biol.* **210**, 1897-1911.

Hedrick, T. L. and Robinson, A. K. (2010). Within-wingbeat damping: dynamics of continuous free-flight yaw turns in *Manduca sexta*. *Biol. Lett.* **6**, 422-425.

Hedrick, T. L., Tobalske, B. W. and Biewener, A. A. (2002). Estimates of circulation and gait change based on a three dimensional kinematic analysis of flight in cockatiels (*Nymphicus hollandicus*) and ringed turtle-doves (*Streptopelia risoria*). *J. Exp. Biol.* **205**, 1389-1409.

Hedrick, T. L., Tobalske, B. W. and Biewener, A. A. (2003). How cockatiels (*Nymphicus hollandicus*) modulate pectoralis power output across flight speeds. *J. Exp. Biol.* **206**, 1363-1378.

Hedrick, T. L., Usherwood, J. R. and Biewener, A. A. (2004). Wing inertia and whole body acceleration: an analysis of instantaneous aerodynamic force production in cockatiels (*Nymphicus hollandicus*) flying across a range of speeds. *J. Exp. Biol.* **207**, 1689-1702.

Hedrick, T. L., Cheng, B. and Deng, X. (2009). Wingbeat time and the scaling of passive rotational damping in flapping flight. *Science* **324**, 252-255.

Hesselberg, T. and Lehmann, F.-O. (2007). Turning behaviour depends on frictional damping in the fruit fly *Drosophila*. *J. Exp. Biol.* **210**, 4319-4334.

Hill, A. (1950). The dimensions of animals and their muscular dynamics. *Sci. Prog.* **38**, 209-230.

Hinterwirth, A. and Daniel, T. (2010). Antennae in the hawkmoth *Manduca sexta* (lepidoptera, sphingidae) mediate abdominal flexion in response to mechanical stimuli. *J. Comp. Physiol. A* **196**, 947-956.

Marden, J. H. and Kramer, M. G. (1994). Surface-skimming stoneflies: a possible intermediate stage in insect flight evolution. *Science*, **266**, 427-430.

Nalbach, G. and Hengstenberg, R. (1994). The halteres of the blowfly *Calliphora*. *J. Comp. Physiol. A* **175**, 695-708.

Pringle, J. W. S. (1948). The gyroscopic mechanism of the halteres of diptera. *Phil. Trans. R. Soc. Lond. B* **233**, 347-384.

Riskin, D. K., Iriarte-Diaz, J., Middleton, K. M., Breuer, K. S. and Swartz, S. M. (2010). The effect of body size on the wing movements of pteropodid bats, with insights into thrust and lift production. *J. Exp. Biol.* **213**, 4110-4122.

Ristroph, L., Bergou, A. J., Ristroph, G., Coumes, K., Berman, G. J., Guckenheimer, J., Wang, Z. J. and Cohen, I. (2010). Discovering the flight autostabilizer of fruit flies by inducing aerial stumbles. *Proc. Natl. Acad. Sci. USA* **107**, 4820-4824.

Ristroph, L., Bergou, A. J., Guckenheimer, J., Wang, Z. J. and Cohen, I. (2011). Paddling mode of forward flight in insects. *Phys. Rev. Lett.* **106**, 178103.

Sane, S. P., Dieudonne, A., Willis, M. A. and Daniel, T. L. (2007). Antennal mechanosensors mediate flight control in moths. *Science* **315**, 863-866.

Sotavalta, O. (1952). The essential factor regulating the wing-stroke frequency of insects in wing mutilation and loading experiments and in experiments at subatmospheric pressure. *Annu. Zool. Soc. Vanamo* **15**, 1-67.

Sotavalta, O. (1954). The effect of wing inertia on the wing-stroke frequency of moths, dragonflies and cockroach. *Annu. Entomol. Fennici* **20**, 93-101.

Stengel, R. F. (2004). *Flight Dynamics*. Princeton, NJ: Princeton University Press.

Taylor, G. K. and Krapp, H. G. (2007). Sensory systems and flight stability: what do insects measure, and why? In *Insect Mechanics and Control*, Vol. 34 (ed. J. Casas and S. J. Simpson), pp. 231-316. London: Academic Press.

Thollesson, M. and Norberg, U. M. (1991). Moments of inertia of bat wings and body. *J. Exp. Biol.* **158**, 19-35.

Thomas, A. L. R. and Taylor, G. K. (2001). Animal flight dynamics. I. Stability in gliding flight. *J. Theor. Biol.* **212**, 399-424.

Tobalske, B. W. and Dial, K. P. (1996). Flight kinematics of black-billed magpies and pigeons over a wide range of speeds. *J. Exp. Biol.* **199**, 263-280.

Tobalske, B. W. and Dial, K. P. (2007). Aerodynamics of wing-assisted incline running in birds. *J. Exp. Biol.* **210**, 1742-1751.

Tobalske, B. W., Peacock, W. L. and Dial, K. P. (1999). Kinematics of flap-bounding flight in the zebra finch over a wide range of speeds. *J. Exp. Biol.* **202**, 1725-1739.

Van den Berg, C. and Rayner, J. M. V. (1995). The moment of inertia of bird wings and the inertial power requirement for flapping flight. *J. Exp. Biol.* **198**, 1655-1664.

Weis-Fogh, T. (1973). Quick estimates of flight fitness in hovering animals, including novel mechanisms for lift production. *J. Exp. Biol.* **59**, 169-230.

Wells, D. J. (1993). Muscle performance in hovering hummingbirds. *J. Exp. Biol.* **178**, 39-57.

Wootton, R. J. and Ellington, C. P. (1991). Biomechanics and the origin of insect flight. In *Biomechanics in Evolution* (ed. J. M. V. Rayner and R. J. Wootton), pp. 99-112. Cambridge, UK: Cambridge University Press.

Yanoviak, S. P., Dudley, R. and Kaspari, M. (2005). Directed aerial descent in canopy ants. *Nature* **433**, 624-626.